

Surfactant Variations in Porous Media Localize Capillary Instabilities during Haines Jumps

Yaniv Edery and David Weitz

John A. Paulson School of Engineering and Applied Sciences, Harvard University, Cambridge, Massachusetts 02138, USA

Steffen Berg

Shell Global Solutions International B.V., Kesslerpark 1, 2288 GS Rijswijk, Netherlands



(Received 10 July 2017; published 12 January 2018)

We use confocal microscopy to measure velocity and interfacial tension between a trapped wetting phase with a surfactant and a flowing, invading nonwetting phase in a porous medium. We relate interfacial tension variations at the fluid-fluid interface to surfactant concentration and show that these variations localize the destabilization of capillary forces and lead to rapid local invasion of the nonwetting fluid, resulting in a Haines jump. These spatial variations in surfactant concentration are caused by velocity variations at the fluid-fluid interfaces and lead to localization of the Haines jumps even in otherwise very uniform pore structure and pressure conditions. Our results provide new insight into the nature of Haines jumps, one of the most ubiquitous and important instabilities in flow in porous media.

DOI: [10.1103/PhysRevLett.120.028005](https://doi.org/10.1103/PhysRevLett.120.028005)

The physical process where an immiscible fluid phase replaces a second resident fluid in a porous medium is inherent in many applications, including soil remediation [1], oil recovery [2], CO₂ sequestration [3], and percolation of coffee [4]. Such fluid flow in porous media is most commonly described by the Darcy equation, which is a mean field description that effectively captures the continuum behavior [5]. However, for multiphase fluid flow, the local wetting behavior of each fluid and the pore-scale dynamics are also essential in determining the flow properties, and these effects must be included in the description of the flow. One important class of fluid flow is drainage, where a nonwetting phase replaces a wetting phase. In drainage, pore-scale dynamics are essential, as capillary forces dominate viscous forces and gravity to drive fluid flow at the scale of individual pores [6,7]. A nonwetting fluid can invade a pore filled with a wetting fluid only when the driving pressure exceeds the capillary pressure at the pore throat. Micromodel experiments, which enable precise visualization of the fluid flow, show that when this capillary pressure is exceeded, the nonwetting fluid invades the pore and continues to flow until it reaches another pore throat where the capillary pressure is sufficiently high to stop further flow [8,9]. This rapid local flow between stable configurations is called a Haines jump [10], and these jumps constitute a key component of the invasion-percolation description of fluid flow in porous media. This forms the basis of quasistatic pore-network modeling and is an important improvement over the mean field description. Despite the ubiquitous occurrence and importance of Haines jumps in flow in porous media, they remain a poorly understood instability. Thus, the decomposition of

the flow into a connected series of Haines jumps is still an inadequate description of the observed flow behavior, as it misses important features such as large burst events that fill dozens of pores in a single step [9,11]. Haines jumps can also occur on isolated oil ganglia in a cooperative, nonlocal process where the capillary forces are different for the leading and trailing menisci, but they are connected by a viscous pressure gradient induced by the fluid flow [8,12]. However, even cooperative interactions cannot account for the common observation that any one specific ganglion can be destabilized while another, very similar one will remain stagnant. Moreover, in 2D micromodels fabricated with very regular pore geometries, Haines jumps can occur seemingly randomly in space and time [8,12,13]. These effects cannot be explained solely by pore geometry variation or by viscous forces; instead chemical variations such as surfactants or impurity concentrations must be present in these systems. This is particularly important in many technical systems where the surfactant concentration is not constant but can instead vary due to changes in pressure, temperature, or chemical composition [14–16]. To fully resolve the complex relation between flow dynamics and chemical composition, detailed pore-scale flow measurements of both the wetting and nonwetting fluids are essential. These can provide the insight required to help understand the very nature of Haines jumps and their apparent randomness [8,17,18] and to distinguish the effects of structural heterogeneity from other contributions [19].

Here, we probe the behavior of Haines jumps for drainage in highly controlled porous media. We use a system where the resident wetting phase is oil and the invading nonwetting phase is water, and we quantify the interfacial interactions

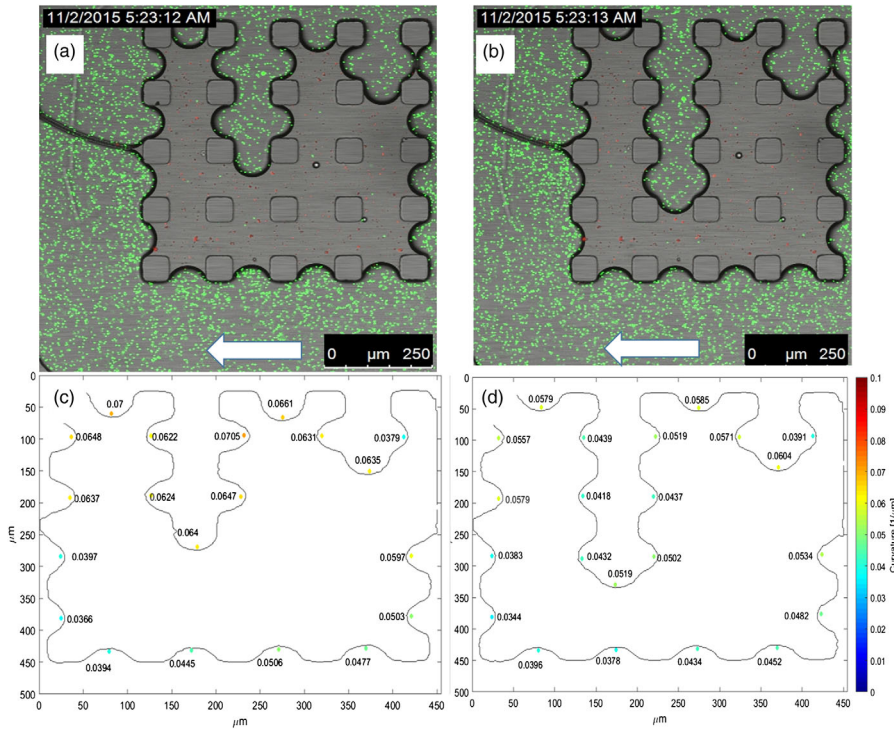


FIG. 1. Trapped oil phase in a 2D porous medium with a 5×5 post array with equal distances of $75 \mu\text{m}$. (a) Trapped oil phase (the red fluorescent beads) before water invasion (the green fluorescent beads). A white arrow marks the flow direction. (b) Trapped oil phase after water invasion into the oil. A white arrow marks the flow direction. (c) Meniscus between water and oil before water advance. The color code corresponds to the curvature value. (d) Meniscus between water and oil after water advance.

in the presence of an added surfactant. Surprisingly, as the local interfacial drag force increases, the local curvature decreases. We show that this inverse relation results from the depletion of surfactant due to the interfacial drag of the invading fluid. This results in local variations of the surface tension, which leads to localizing capillary instabilities that drive the Haines jumps to occur in specific pores, whereas similar pores remain stagnant otherwise.

We use a 2D microfluidic model porous medium fabricated from a thiolene-based prepolymer (NOA 81) polymerized on a polydimethylsiloxane slab. The device dimensions are $1000 \times 1000 \times 50 \mu\text{m}^3$, and square, $50 \mu\text{m}^3$ posts are arranged in a 5×5 array with uniform spacing, as seen in Figs. 1(a) and 1(b). The array of posts creates a series of pore throats formed by the narrowest area that connect the adjacent pores. The device is hydrophobic, with a water-air contact angle of 110° ; hence, oil is the wetting phase, while water is the nonwetting phase. A ganglion of trapped oil at the posts is replaced by water, mimicking a drainage process into an isolated wetting phase ganglion trapped in a porous medium. The post array is positioned at the center of the flow cell, leaving channels on either side through which water flows along the paths of least resistance. Three different uniform post spacings are employed, 50, 75, and $100 \mu\text{m}$, with three different flow rates, $Q = 1, 10, 100 \mu\text{l/h}$, used for each spacing. The oil is mineral oil with a viscosity of 16.8 cP, and the water is double distilled to ensure that there are no salt ions in the water to interact with the surfactant in the oil. Fluorescent beads are used to trace the flow of oil and water. Nile red fluorescent beads are suspended in the oil phase using

0.5 wt % surfactant (ABIL EM 90); the interfacial tension between water and oil with this surfactant concentration is $\sigma = 12.6 \text{ mN/m}$. The beads are $1 \mu\text{m}$ in diameter and are diluted to 10^{-4} wt % of the oil. Yellow-green latex fluorescent beads are suspended in the water phase; these beads are $5 \mu\text{m}$ in diameter. In all experiments the oil is trapped in the post array, while the water flows freely around it.

Visualization is performed using confocal microscopy with a $10 \times$ lens with a NA of 0.4; this provides a larger field of view, while the wide confocal aperture allows all planes to be in focus. A 488 nm laser excites the fluorescent beads; the Nile red beads emit at a wavelength of 650 nm, while the yellow-green beads emit at 514 nm, thus differentiating the two fluid phases. The corresponding colors in Figs. 1(a) and 1(b) are red and green, respectively, for easy differentiation. Analysis is done using a particle image velocimetry (PIV) program [20] to correlate particle displacements between consecutive images, taken every 100 msec; from this, a velocity and direction map for the oil and water phase can be formed as shown in Fig. 2. Menisci between oil, water, and the solid medium are traced and analyzed by MATLAB to calculate the volume and curvature changes in time, as shown in Figs. 1(c) and 1(d). Using this protocol we determine the drag forces across the water-oil interface, the local capillary pressures, and the local curvatures.

The experiment begins with an oil ganglion trapped in the post array, with the water flowing around it, in the adjacent channels. The water-oil interfaces always form curved menisci due to capillary forces; these interfaces are seen as black lines in the confocal images in Fig. 1. A thin

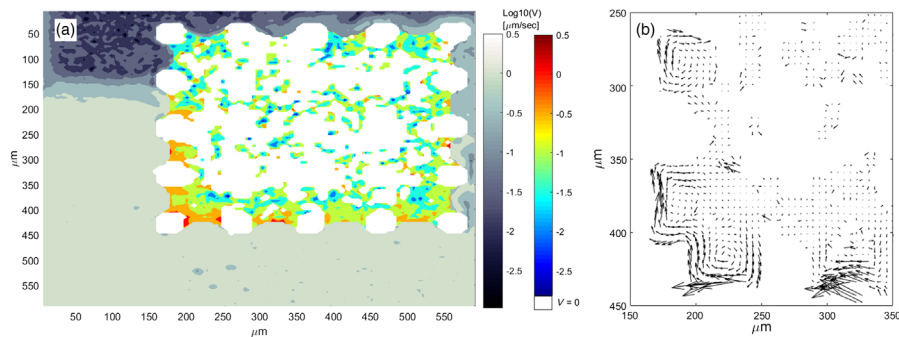


FIG. 2. (a) Velocity map of the two phases in the 2D experiment averaged over time; gray scale is the water phase velocity, while RGB is the oil phase measured velocity. (b) Direction map of the oil ganglion marked by arrows. The directional arrows show circulation in the oil due to interfacial drag forces applied by the water phase.

film stretches from the oil ganglion to the outlet wall of the cell, displayed as the black line. Interfacial drag forces of the water on the oil continuously extract oil from the ganglion through the thin film; it also separates the flow fields of the water on either side of the ganglion. However, the volume of the oil seems unaffected by the steady outflow of oil until a sudden rapid advance of water penetrates a single individual pore; this is a Haines jump. The seemingly randomly located water advance requires an increase in Laplace pressure to overcome the local capillary pressure at that specific pore.

The Haines jumps are investigated locally at each meniscus by tracking the Laplace pressure. The steady outflow of oil through the thin film decreases the pressure within the oil ganglion, and water enters each of the throats between the pillars surrounding the ganglion, accommodating the volume reduction of the oil, as seen in Fig. 1 and in movie 1 of the Supplemental Material (SM) [21]. This advancement pattern is accompanied by a steady increase in the curvatures at the water-oil menisci as the Laplace pressure changes due to the decreasing volume of the oil ganglion. By tracking this change in shape in all of the menisci and transforming curvatures to capillary pressure using the Young-Laplace equation, we determine a mean capillary pressure for the water-oil interface. The average capillary pressure rises steadily in all pore throats as oil is drawn out from the ganglion and then drops precipitously as water invades a single localized pore, as shown by the blue curve in Fig. 3. Although all pore throats are equal in size, water advances only in a specific pore—and only one pore at a time. The sudden drop in the average Laplace pressure corresponds exactly to water invading a single pore, as shown in Figs. 1(a) and 1(b), respectively, where water (marked in green) penetrates a single pore previously occupied with oil (marked in red). The invaded pore volume is much larger than the volume of the curvature change at the interface; thus, there is a marked receding of the water in all of the throats around the oil ganglion, as can be seen by comparing the position at the interfaces before and after the Haines jump in Figs. 1(a) and 1(b) and in movie 1 of the SM [21]. The period of the Haines jumps is very regular and is about 100 sec, in close agreement with

the value estimated from a calculation of the outward flux by the oil through the thin film determined using a Couette-flow approximation.

If the experiment is repeated using the same geometry and flow conditions, a similar pattern of advancing water is observed. The Haines jumps all occur on the side where the water flow is low; however, the exact pattern by which they advance can vary from run to run. Similarly, experiments with other pore sizes and different flow rates also lead to the same behavior, with the Haines jumps all occurring where the water flow was the slowest but following slightly different specific patterns of advancements each time, as seen in movies 2 and 3 of the SM [21].

To understand why a Haines jump is localized at a single pore throat, we measure the curvature of each meniscus and list the values in Figs. 1(c) and 1(d). The curvatures are systematically larger, by 30%, on the side on which a Haines jump occurs than on the opposite side. The spatially correlated variations reflect pore-to-pore correlations of either the Laplace pressure or the interfacial tension. The internal pressure within the oil must be spatially uniform, as there is no indication of flow within the ganglion, as shown by both the PIV measurement of the flow velocity and the direction map within the oil, which are depicted in Figs. 2(a) and 2(b), respectively. In addition, the pressure of the water is essentially constant on both sides; the difference due to the flow rate is orders of magnitude less than the typical Laplace pressure, as shown in the SM [21]. Thus, the Laplace pressure must be constant, and the variation in curvature must instead be due to a change in the surface tension of the water-oil interface in each meniscus. The observed decrease in local curvature must be due to an increase in interfacial tension, and this in turn must be due to a decrease in surfactant concentration, as seen in Fig. 3 (the red line). The Haines jump occurs where the relative interfacial tension is lowest. To quantify the change in surfactant concentration, we use a pendant-drop technique to measure the scaling between surfactant concentration and curvature for the liquids and surfactant used in the experiment [22,23]. We then make the assumption that the same relative change in curvature of the interface in the porous media results from the same change in surfactant

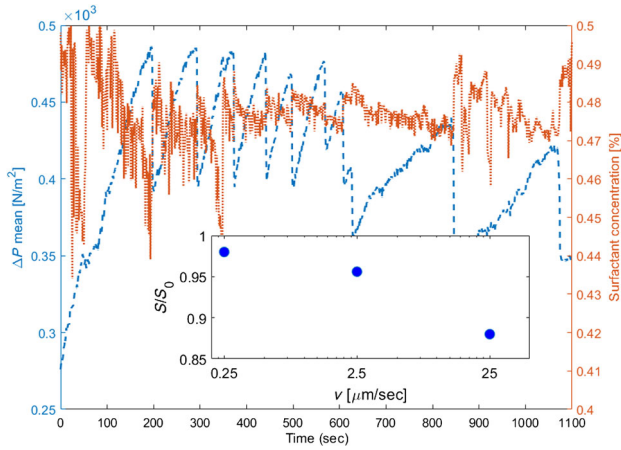


FIG. 3. Blue line correlates the mean capillary pressure in time between oil and water as calculated from the curvature. The red line is the surfactant concentration on the water-oil interface adjacent to the flowing channel where the surfactant is depleted. (Inset) Normalized surfactant concentration on the interface of oil and water near the flowing channel.

concentration. We further assume that the surfactant concentration is saturated at the interface with the maximum curvature. We can thus determine the surfactant concentration at each interface. There is a marked inhomogeneity in surfactant concentration along the menisci. The most pronounced difference is the large decrease in surfactant concentration between the menisci on either side of the oil ganglion, as seen in Fig. 3; this corresponds directly to the differences in curvature of the menisci on either side, as seen in Fig. 1. The main difference between the menisci on the two sides of the oil ganglion is the flow of the water in the larger channels. From the pendant-drop measurements, we can infer the local surfactant concentration by rescaling the measured local curvatures by the maximum value of the curvature determined at saturated surfactant concentration. The spatial variation of flow on the water-oil interface can be seen in the PIV data; see Fig. 2(a). The water is nearly stagnant in the channel adjacent to where the jumps occur, marked in dark gray, whereas there is uniformly high flow in the channel on the other side of the oil ganglion, marked by light gray. The high flow of the water exerts an interfacial drag force on the adjacent menisci and, as shown in Fig. 2(b) and in movie 1 of the Supplemental Material [21], this leads to a depletion of the surfactant. Thus, the variation in local curvature of the menisci results primarily from changes in the local flow of the fluid surrounding the oil ganglion, as highlighted by the red line in Fig. 3. Moreover, this also leads directly to the localization of the Haines jumps, which results from the spatial variation of the surfactant concentration; at significantly lower surfactant concentration, these spatial variations are no longer observed and the localization effect disappears (see movie 4 and the discussion in the SM [21]).

To confirm that the local surfactant concentration is controlled by a flow of the water adjacent to the oil ganglion, we investigate the change in concentration as the flux of the water flow is varied. We average the surfactant concentration on the interfaces over the entire experiment and normalize by the saturation value. On the side where the water is flowing rapidly, there is a measurable decrease as the water flux increases; by contrast, by the side where the water is stagnant, there is very little change, as shown in Fig. 3. Thus, higher flow rates of the water lead to a lower surfactant concentration. This is further corroborated by the variation in surfactant concentration on the menisci along the interface of the side of the oil ganglion where the water flows faster. The curvature of the menisci decreases from the side where the water enters to the side where it exits, as seen going from right to left on the bottom of Fig. 1. The origin of this decrease must come from the increased flow of the water; this is most apparent at the increased speed of the oil at the interface of the menisci, as shown in Figs. 2(a) and 2(b). The flow of the water must sweep the surfactant from the interface exposing fresh oil. From the measurement of the time evolution of the surface tension using the pendant-drop technique, we know that it requires on the order of an hour to fully recover on a bare surface. Thus, the more rapid the flow, the lower the concentration of surfactant and hence the larger the surface tension, accounting for the observed change in curvature of the menisci on the lower interface, where there is a rapid flow of water (as seen in the inset of Fig. 3). This confirms that the local surfactant concentration is controlled by the flow of the adjacent water.

The results reported in this Letter show the importance of local variations in the velocity of the displacing fluid which can directly drive variations in surfactant concentration, and thus in surface tension. The result is local variations in Laplace pressure, and it is these variations that ultimately determine where a Haines jump occurs. Thus, even in a very uniform porous medium, the Haines jumps are still highly localized. These effects should also occur in real 3D porous media, such as rock formations, soil, and coffee grounds; in that case, however, heterogeneity will further exacerbate the velocity variation of ganglia of the resident fluid. As such, inhomogeneous depletion of the surfactant will be more pronounced, enhancing the localization of Haines jumps when they occur. Haines jumps can even occur on a totally stagnant ganglion; the displacement of the resident fluid by the displacing fluid at the Haines jump, however, must be compensated for by the flow of the resident fluid into a new location, leading to transport of the whole ganglion. These effects may also offer a rationalization for the widely observed persistence of Haines jumps in oil recovery long after steady state flow has been achieved; in these cases the surfactant is in the invading fluid, and the continuum flow of this fluid can lead to a slow evolution of the surfactant concentration on the

menisci, resulting in the persistence of the Haines jumps. Furthermore, in many cases surfactants can be produced within the porous medium; this frequently happens, for example, in enhanced oil recovery, where surface active molecules occur naturally in the oil and can produce surfactants through interactions between the displacing fluid and the rock formation. All of these effects will profoundly affect both the location of the Haines jumps and the displacement of the resident fluid, and they must be included in any pore-scale modeling of the fluid flow. The results presented here provide guidance for doing so.

This work was supported partially by the MRSEC program of the National Science Foundation under Grant No. DMR-1420570 and by the National Science Foundation (Grants No. DMR-1708729 and No. DMR-1611089). This work was performed in part at the Center for Nanoscale Systems (CNS), a member of the National Nanotechnology Coordinated Infrastructure Network (NNCI), which is supported by the National Science Foundation under NSF Grant No. 1541959. CNS is part of Harvard University. Y. E. gratefully acknowledges fellowship support from the Israel Ministry of Energy and Water.

-
- [1] Y. B. Acar and A. N. Alshwabkeh, Principles of electrokinetic remediation, *Environ. Sci. Technol.* **27**, 2638 (1993).
- [2] D. O. Shah, *Improved Oil Recovery by Surfactant and Polymer Flooding* (Elsevier, New York, 2012).
- [3] C. R. Jenkins, P. J. Cook, J. Ennis-King, J. Undershultz, C. Boreham, T. Dance, P. de Caritat, D. M. Etheridge, B. M. Freifeld, A. Hortle, D. Kirste, L. Paterson, R. Pevzner, U. Schacht, S. Sharma, L. Stalker, and M. Urosevic, Safe storage and effective monitoring of CO₂ in depleted gas fields, *Proc. Natl. Acad. Sci. U.S.A.* **109**, E35 (2012).
- [4] A. Fasano and M. Primicerio, in *Calculus of Variations, Applications and Computations*, edited by C. Bandle, J. Bemelmans, M. Chipot, J. Saint Jean Paulin, and I. Shafrir, Pitman Research Notes in Mathematics Series Vol. 326 (Chapman and Hall, London, 1995), p. 109.
- [5] J. Bear, *Dynamics of Fluids In Porous Media*, Vol. 1 (American Elsevier, New York, 1972).
- [6] R. Lenormand, C. Zarcone, and A. Sarr, Mechanisms of the displacement of one fluid by another in a network of capillary ducts, *J. Fluid Mech.* **135**, 337 (1983).
- [7] R. Hilfer and P. E. Øren, Dimensional analysis of pore scale and field scale immiscible displacement, *Transp. Porous Media* **22**, 53 (1996).
- [8] R. T. Armstrong and S. Berg, Interfacial velocities and capillary pressure gradients during Haines jumps, *Phys. Rev. E* **88**, 043010 (2013).
- [9] S. Berg, H. Ott, S. A. Klapp, A. Schwing, R. Neiteler, N. Brussee, A. Makurat, L. Leu, F. Enzmann, J.-O. Schwarz *et al.*, Real-time 3D imaging of Haines jumps in porous media flow, *Proc. Natl. Acad. Sci. U.S.A.* **110**, 3755 (2013).
- [10] W. B. Haines, Studies in the physical properties of soil. V. The hysteresis effect in capillary properties, and the modes of moisture distribution associated therewith, *Journal of agricultural science* **20**, 97 (1930).
- [11] S. Berg, R. T. Armstrong, H. Ott, A. Georgiadis, S. A. Klapp, A. Schwing, R. Neiteler, N. Brussee, A. Makurat, L. Leu, F. Enzmann, J.-O. Schwarz, M. Wolf, F. Khan, M. Kersten, S. Irvine, and M. Stampanoni, in *Proceedings of the International Symposium of the Society of Core Analysts*, Napa Valley, CA, (Society of Core Analysts, Rusa-gonis, Canada, 2013), paper SCA2013-011, <http://www.jgmaas.com/SCA/2013/SCA2013-011.pdf>.
- [12] M. Rücker, S. Berg, R. T. Armstrong, A. Georgiadis, H. Ott, A. Schwing, R. Neiteler, N. Brussee, A. Makurat, L. Leu *et al.*, From connected pathway flow to ganglion dynamics, *Geophys. Res. Lett.* **42**, 3888 (2015).
- [13] H. Yuan and B. F. Swanson, Resolving pore-space characteristics by rate-controlled porosimetry, *SPE Form. Eval.* **4**, 17 (1989).
- [14] W. Xu, S. C. Ayirala, and D. N. Rao, Compositional dependence of wetting and contact angles in solid-liquid-liquid systems under realistic environments, *Can. J. Chem. Eng.* **84**, 44 (2006).
- [15] J. S. Buckley and T. Fan, Crude oil/brine interfacial tensions, *Petrophysics* **48**, 175 (2007).
- [16] W. Xu, S. C. Ayirala, and D. N. Rao, Measurement of surfactant-induced interfacial interactions at reservoir conditions, *SPE Reservoir Eval. Eng.* **11**, 83 (2006).
- [17] M. Andrew, B. Bijeljic, and M. J. Blunt, Pore-by-pore capillary pressure measurements using x-ray microtomography at reservoir conditions: Curvature, snap-off, and remobilization of residual CO₂, *Water Resour. Res.* **50**, 8760 (2014).
- [18] K. Singh, B. Bijeljic, and M. J. Blunt, Imaging of oil layers, curvature and contact angle in a mixed-wet and a water-wet carbonate rock, *Water Resour. Res.* **52**, 1716 (2016).
- [19] G. R. Jerauld and S. J. Salter, The effect of pore-structure on hysteresis in relative permeability and capillary pressure: Pore-level modeling, *Transp. Porous Media* **5**, 103 (1990).
- [20] W. Thielicke and E. J. Stamhuis, PIVLAB towards user-friendly, affordable and accurate digital particle image velocimetry in MATLAB, *J. Open Res. Software* **2**, e30 (2014).
- [21] See Supplemental Material at <http://link.aps.org/supplemental/10.1103/PhysRevLett.120.028005> for movies and additional derivations.
- [22] J. Drelich, C. H. Fang, and C. L. White, Measurement of interfacial tension in fluid-fluid systems, *Encycl. Surf. Colloid Sci.* **3**, 3158 (2002).
- [23] H. Lee, C.-H. Choi, A. Abbaspourrad, C. Wesner, M. Caggioni, T. Zhu, S. Nawar, and D. A. Weitz, Fluorocarbon oil reinforced triple emulsion drops, *Adv. Mater.* **28**, 8425 (2016).